

# UCSF

## UC San Francisco Previously Published Works

### Title

Serine ubiquitination of SQSTM1 regulates NFE2L2-dependent redox homeostasis.

### Permalink

<https://escholarship.org/uc/item/2z60w0cr>

### Journal

Autophagy, 21(2)

### Authors

Mukherjee, Rukmini  
Bhattacharya, Anshu  
Mello-Vieira, Joao  
et al.

### Publication Date

2025-02-01

### DOI

10.1080/15548627.2024.2404375

Peer reviewed

## Serine ubiquitination of SQSTM1 regulates NFE2L2-dependent redox homeostasis

Rukmini Mukherjee<sup>a,b,c</sup>, Anshu Bhattacharya<sup>a,b</sup>, João Mello-Vieira<sup>a,b</sup>, Santosh Kumar Kuncha<sup>a,b</sup>, Marina Hoffmann<sup>a</sup>, Alexis Gonzalez<sup>a</sup>, Rajeshwari Rathore<sup>a</sup>, Attinder Chadha<sup>d,e</sup>, Donghyuk Shin<sup>b,f</sup>, Thomas Colby<sup>g</sup>, Ivan Matic<sup>g,h</sup>, Shaeri Mukherjee<sup>d,e,i</sup>, Mohit Misra<sup>a,b</sup>, and Ivan Dikic <sup>a,b,c,j</sup>

<sup>a</sup>Institute of Biochemistry II, Faculty of Medicine, Goethe University, Frankfurt, Germany; <sup>b</sup>Molecular Signaling, Goethe University, Frankfurt, Germany; <sup>c</sup>Biophysics, Max Planck Institute of Biophysics, Frankfurt, Germany; <sup>d</sup>Department of Microbiology and Immunology, University of California, San Francisco, California, USA; <sup>e</sup>The George William Hooper Foundation, University of California, San Francisco, USA; <sup>f</sup>Department of Systems Biology, College of Life Science and Biotechnology, Yonsei University, Seoul, Republic of Korea; <sup>g</sup>Max Planck Institute for Biology of Ageing, Cologne, Germany; <sup>h</sup>CECAD Cluster of Excellence, University of Cologne, Cologne, Germany; <sup>i</sup>Chan Zuckerberg Biohub, San Francisco, USA; <sup>j</sup>Translational Medicine and Pharmacology, Fraunhofer Institute for Translational Medicine and Pharmacology (ITMP), Frankfurt, Germany

### ABSTRACT

The KEAP1-NFE2L2 axis is essential for the cellular response against metabolic and oxidative stress. KEAP1 is an adaptor protein of CUL3 (cullin 3) ubiquitin ligase that controls the cellular levels of NFE2L2, a critical transcription factor of several cytoprotective genes. Oxidative stress, defective autophagy and pathogenic infections activate NFE2L2 signaling through phosphorylation of the autophagy receptor protein SQSTM1, which competes with NFE2L2 for binding to KEAP1. Here we show that phosphoribosyl-linked serine ubiquitination of SQSTM1 catalyzed by SidE effectors of *Legionella pneumophila* controls NFE2L2 signaling and cell metabolism upon *Legionella* infection. Serine ubiquitination of SQSTM1 sterically blocks its binding to KEAP1, resulting in NFE2L2 ubiquitination and degradation. This reduces NFE2L2-dependent antioxidant synthesis in the early phase of infection. Levels of serine ubiquitinated SQSTM1 diminish in the later stage of infection allowing the expression of NFE2L2-target genes; causing a differential regulation of the host metabolome and proteome in a NFE2L2-dependent manner.

**Abbreviation:** ARE: antioxidant response element; Dup: deubiquitinase specific for phosphoribosyl-linked serine ubiquitination; ER: endoplasmic reticulum; h.p.i: hours post infection; HIF1A/HIF-1 $\alpha$ : hypoxia inducible factor 1 subunit alpha; KEAP1: kelch like ECH associated protein 1; KIR: KEAP1-interacting region; LIR: LC3-interacting region; NES: nuclear export signal; NF $\kappa$ B/NF- $\kappa$ B: nuclear factor kappa B; NLS: nuclear localization signal; NFE2L2/Nrf2: NFE2 like bZIP transcription factor 2; PB1 domain: Phox1 and Bem1 domain; PR-Ub: phosphoribosyl-linked serine ubiquitination; ROS: reactive oxygen species; SQSTM1/p62: sequestosome 1; tBHQ: tertiary butylhydroquinone; TUBE2: tandem ubiquitin binding entity 2; UBA domain: ubiquitin-associated domain.

### ARTICLE HISTORY

Received 3 April 2023  
Revised 10 September 2024  
Accepted 11  
September 2024

### KEYWORDS



Antioxidants; bacterial infection; KEAP1; legionella pneumophila; oxidative stress; reactive oxygen species


## Introduction

Reactive oxygen species (ROS) are important to maintain redox homeostasis in the cell. Free radicals like hydroxyl (OH $\cdot$ ), superoxide (O $_2^{\cdot-}$ ), nitric oxide (NO $\cdot$ ), nitrogen dioxide (NO $_2\cdot$ ), peroxy (ROO $\cdot$ ) and lipid peroxy (LOO $\cdot$ ) are generated in enzymatic reactions in cellular compartments which alter the redox state of the cell. Oxidative stress arising from high ROS levels activate redox-sensitive transcriptional factors including the NFE2L2 (NFE2 like bZIP transcription factor 2) which produce antioxidants to restore the redox state of the cell. Under homeostatic conditions, nuclear levels of NFE2L2 are kept low by its cytosolic repressor KEAP1 (kelch like ECH associated protein 1) which is a substrate adapter protein for the CUL3 (cullin 3)-RBX1 (ring-box 1) E3-ubiquitin ligase system. KEAP1 targets NFE2L2 for ubiquitination and proteasomal degradation. Under oxidative stress, specific cysteines on KEAP1 are oxidized, leading to conformational changes which release the KEAP1-bound NFE2L2,

allowing it to translocate to the nucleus where it heterodimerizes with sMAF (small musculoaponeurotic fibrosarcoma protein), binds to promoters with antioxidant response elements (AREs) to drive the transcription of NFE2L2-target genes [1].

Redox signaling is closely associated with cellular metabolism and autophagy. The direct interaction between the autophagy receptor protein SQSTM1/p62 (sequestosome 1) and KEAP1 links autophagy to NFE2L2 signaling. SQSTM1 is a multifunctional protein with several domains, including a Phox1 and Bem1 (PB1) domain, a zinc finger (ZZ), two nuclear localization signals (NLSs), a TRAF6 binding (TB) domain, a nuclear export signal (NES), an LC3-interacting region (LIR), a KEAP1-interacting region (KIR), and an ubiquitin-associated (UBA) domain. SQSTM1 is well-known for its role in selective autophagy of ubiquitinated cargo comprising intracellular bacteria, depolarized mitochondria or ubiquitinated protein aggregates [2–4]. Binding of SQSTM1 to

**CONTACT** Ivan Dikic  [idikic@biochem2.uni-frankfurt.de](mailto:idikic@biochem2.uni-frankfurt.de)  Institute of Biochemistry II, University Hospital Building 75, Theodor-Stern-Kai 7, Frankfurt 60590, Germany

 Supplemental data for this article can be accessed online at <https://doi.org/10.1080/15548627.2024.2404375>

© 2024 The Author(s). Published by Informa UK Limited, trading as Taylor & Francis Group.  
This is an Open Access article distributed under the terms of the Creative Commons Attribution-NonCommercial-NoDerivatives License (<http://creativecommons.org/licenses/by-nc-nd/4.0/>), which permits non-commercial re-use, distribution, and reproduction in any medium, provided the original work is properly cited, and is not altered, transformed, or built upon in any way. The terms on which this article has been published allow the posting of the Accepted Manuscript in a repository by the author(s) or with their consent.

ubiquitinated cargo is facilitated by phosphorylation of specific serine residues in its UBA domain (S403, S407). Upon binding to ubiquitinated cargo, S351 within the KIR motif of SQSTM1 gets phosphorylated, increasing the binding affinity of its KIR motif to KEAP1. KEAP1 binding to SQSTM1 destabilizes the KEAP1-NFE2L2 interaction, causing NFE2L2 stabilization and its nuclear translocation [5–7]. SQSTM1 can form higher order structures like oligomers and helical filaments and undergo liquid-liquid phase transition forming SQSTM1 bodies and SQSTM1 gels which are sites of autophagosome biogenesis and NFE2L2-dependent antioxidant signaling [8–10].

Bacterial infections alter redox metabolism in the host cell and can activate NFE2L2-dependent antioxidant signaling. NFE2L2 activation can be protective for the host in some cases. For example, *Salmonella typhimurium* infection activates transcription of the NFE2L2-target gene *SLC40A1/Ferroportin-1* (solute carrier family 40 member 1) which is a cellular iron exporter. This limits *Salmonella* access to iron, restraining its intracellular proliferation [11]. *Salmonella* infection also causes phosphorylation of SQSTM1 at S351 on the *Salmonella* containing vacuole, facilitating interaction with KEAP1 and activation of xenophagy [6]. In infections with uropathogenic *Escherichia coli* (UPEC), NFE2L2 activation in urothelial cells reduces ROS generation, inflammation, and promotes UPEC expulsion, therefore reducing the bacterial load. Pharmacological activation of NFE2L2 by sulfaphane causes resistance to *Pseudomonas aeruginosa* in mice [12]. NFE2L2 signaling is also activated to control tissue damage for example in lung damage induced by *Staphylococcus aureus* infections [13]. Some bacteria like *Coxiella burnetii* exploit NFE2L2 to promote intracellular growth. The pathogen stabilizes SQSTM1, causing increase in its phosphorylation that activates NFE2L2 signaling promoting bacterial growth in macrophages [14]. *Mycobacterium tuberculosis* infection also causes an upregulation of NFE2L2-dependent gene expression thus promoting bacterial persistence in alveolar macrophages [15].

*Legionella pneumophila* infection has been associated with an increase in mitochondrial fragmentation and production of mitochondrial ROS, which was partially dependent on the bacterial effector protein MitF. We found phosphoribosyl-linked serine ubiquitination (PR-Ub) catalyzed by the SidE effector proteins to be an important determinant of redox metabolism in infected cells. During infection, SdeA, SdeB, SdeC and SidE mediate attachment of PR-Ub to the serine residues of substrate proteins [16–18]. SdeA is structurally and mechanistically well-studied [19–21]. PR-Ub levels in infected cells are regulated by the action of PR-Ub specific deubiquitinases DupA and DupB [22]. SdeA activity is fine-tuned by the *Legionella* glutamylase SidJ, which inhibits SdeA catalytic activity [23–25]. PR-Ub has been linked to fragmentation of the RTN4-labeled tubular endoplasmic reticulum (ER), and to fragmentation of the Golgi body in *Legionella*-infected cells [16,18,26].

Proteomic analysis showed SQSTM1 to be a putative substrate of PR-Ub during *Legionella* infection. This suggested that autophagy may be regulated by PR-Ub of SQSTM1. However, *Legionella pneumophila* has a sophisticated mechanism to block the formation of autophagosomes using the bacterial effector

protein RavZ, which irreversibly delipidates Atg8-family proteins on phagophore and autophagosomal membranes [27,28]. This study shows how serine ubiquitination of SQSTM1 affects redox metabolism through its regulation of the SQSTM1-KEAP1-NFE2L2 signaling axis. Using a combination of bacterial infection studies, biochemical experiments, and proteomics we have identified the PR-Ub site and dissected the molecular mechanism by which serine ubiquitination of SQSTM1 controls KEAP1-mediated NFE2L2 ubiquitination and degradation without affecting SQSTM1 phosphorylation. This mechanism results in a temporal regulation of redox metabolism in *Legionella* infected cells and leads to NFE2L2-dependent remodeling of the host cell metabolome and proteome, which favor bacterial proliferation under oxidative stress.

## Results

### Mapping of serine ubiquitination sites in SQSTM1 during legionella infection

Previous proteomic data revealed that SQSTM1 is PR-ubiquitinated in *Legionella*-infected cells [22]. In order to validate the PR ubiquitination of endogenous SQSTM1 upon *Legionella* infection a GST pulldown assay was performed by incubating cell lysates from *Legionella* infected cells with the trapping mutant of DupA (GST-DupA[H67A]) followed by western blotting with antibodies against SQSTM1, GST and ubiquitin.  $\Delta D$  ( $\Delta$ DupA/B) *Legionella* infected cells had higher amounts of PR-Ub-modified SQSTM1 compared to WT *Legionella* infected cells. *Legionella* strains lacking SidE enzymes ( $\Delta S$ ) are PR-Ub deficient. The SQSTM1 antibody used is efficient to detect both unmodified and PR-Ub-modified forms of SQSTM1 (Figure 1A). In addition, in order to identify the serine sites of SQSTM1 that are ubiquitinated we subjected purified maltose binding protein (MBP)-tagged SQSTM1 to *in vitro* PR/ubiquitination reaction with SdeA, ubiquitin and NAD and the reaction products of this assay were subjected to mass spectrometry. High-resolution electron-transfer dissociation (ETD) spectra of PR-ubiquitinated peptides identified serines S361 and S365 on SQSTM1 to be modified by PR-Ub (Figure 1B). Based on the domain organization of the protein, it was noted that the identified PR-Ub sites of SQSTM1 were present in the unstructured loop between the KEAP1 interaction region (KIR) and the Ub-associated (UBA) domains (Figure 1B). Mutation of three serine residues at S361, S365, S366 was necessary and sufficient to generate a PR-Ub-deficient mutant of MYC-SQSTM1 (SQSTM1<sup>S361,S365,S366A</sup>) which was not PR-Ub modified upon bacterial infection (Figure 1C). His-tagged SQSTM1 peptide (comprising amino acids 321–440) was PR-Ub modified in an *in vitro* reaction, treated with or without GST-DupA, run on SDS-PAGE and stained with Coomassie Brilliant Blue. *In vitro* PR-Ub resulted in 2 bands separated by ~ 8 kDa corresponding to SQSTM1(321–440) modified on one or different serines (SQSTM1-PR-Ub, SQSTM1-PR-Ub(2×)). Treatment with functional GST-DupA enzyme removed the PR-Ub from the SQSTM1 peptide proving that the modification on SQSTM1 was PR-Ub (Figure S1A).

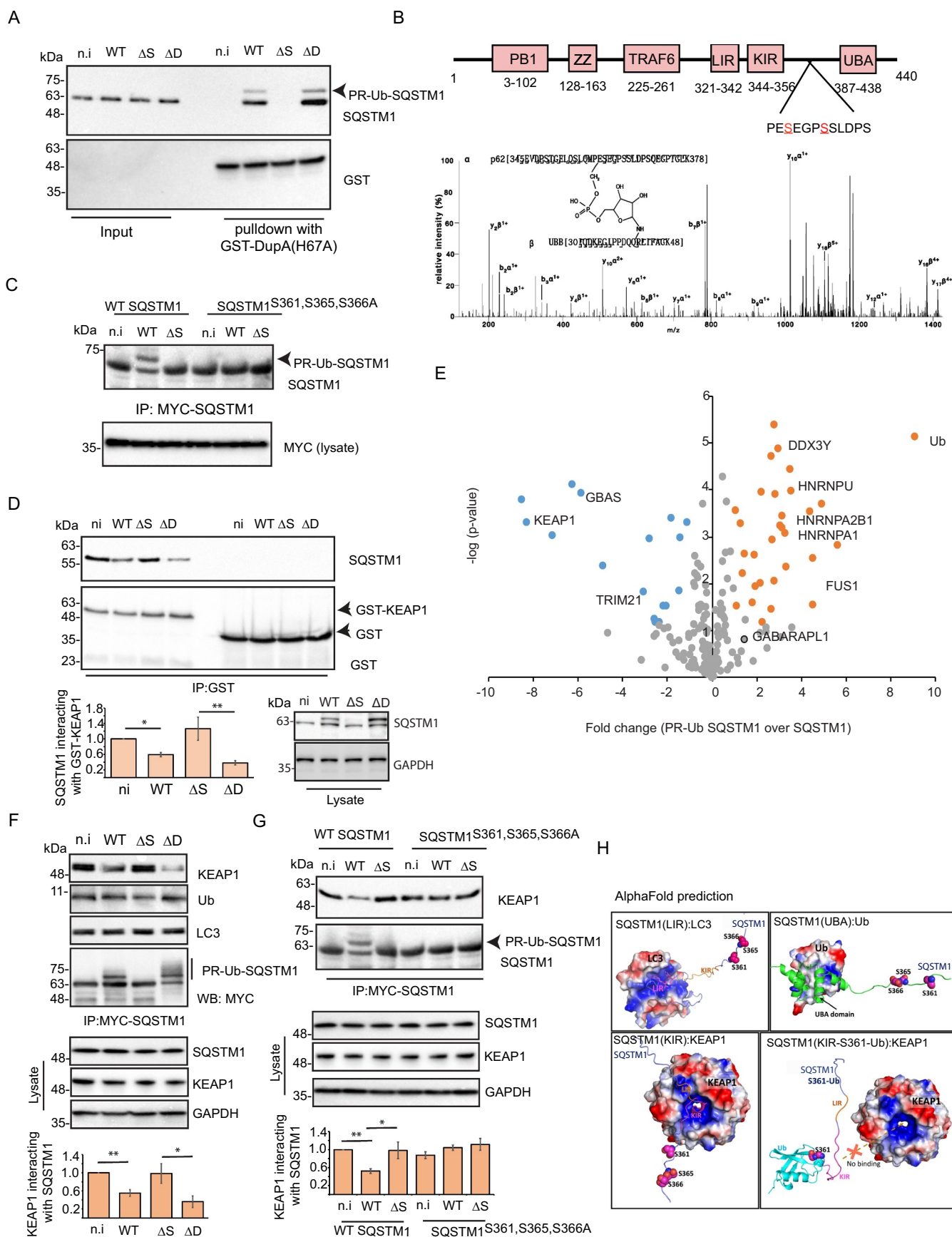


**Figure 1.** PR-Ub of SQSTM1 in legionella infection reduced its interaction with KEAP1. (A) HEK 293T cells expressing CD32 were infected with different strains of legionella for 2 h. Lysates were used for GST affinity isolation with the DupA trapping mutant GST-DupA(H67A), followed by western blots with antibodies against SQSTM1, and GST. This experiment was repeated three times with similar results. (B) Domains of SQSTM1 and identification of site of PR-Ub. (C) HEK293T cells were transfected with myc-tagged wild type or serine ub-deficient SQSTM1 (SQSTM1S361,365,366A) and infected with legionella for 2 h, followed by immunoprecipitation with MYC resin and western blotting. This experiment was repeated three times with similar results. (D) Lysates from cells infected with legionella for 2 h were

### PR-Ub of SQSTM1 partially inhibited its interaction with KEAP1

Since the identified PR-Ub site was in proximity of the LIR, KIR and UBA domains of SQSTM1 we checked whether interaction of SQSTM1 with any of these interactors was affected by its PR-Ub. GST-tagged ubiquitin and LC3 interacted with PR-Ub-modified SQSTM1 (Figure S1B), but GST-KEAP1 showed reduced interaction with PR-Ub SQSTM1 in WT and  $\Delta D$  Legionella infected lysates (Figure 1D). Next, we purified a peptide spanning amino acids 321–400 of SQSTM1 from *E. coli*, PR-ubiquitinated it in an *in vitro* reaction and incubated it with cell lysate from HEK293T cells infected with Legionella in a GST affinity-isolation assay, followed by mass spectrometric identification of interactors. Upon PR-ubiquitination, SQSTM1 (321–400) bound significantly less KEAP1 supporting the data in Figure 1D. We also saw a significant enrichment of several proteins involved with RNA metabolism, HDACs and DNA damage related proteins which preferentially bound to PR-Ub-modified SQSTM1 peptide (Figure 1E and S1C), which will be validated by utilizing the full-length protein in a follow up study.

To test for the interaction between SQSTM1 with KEAP1 in cells we used MYC-SQSTM1 expressing A549 cells infected with wild-type and mutant Legionella strains for 2 h to enrich modified MYC-SQSTM1 and checked for co-precipitation with KEAP1. PR-Ub-modified SQSTM1 present in WT and  $\Delta D$  infected cells bound to less KEAP1 when compared to uninfected or  $\Delta S$  infected cells (Figure 1F). This difference in SQSTM1-KEAP1 interaction between WT and  $\Delta S$  Legionella infection was insignificant when the PR-Ub-deficient mutant of SQSTM1 (SQSTM1<sup>S361,S365,S366A</sup>) was used (Figure 1G). In order to understand the structural basis of how serine ubiquitination of SQSTM1 alters binding to its interaction partners we performed AlphaFold-based complex prediction of LIR, KIR and UBA domains of SQSTM1 with LC3, KEAP1 and ubiquitin, respectively. As expected, the complexes predicted were well in agreement with already existing crystal structures of LIR with LC3 (PDB ID: 2ZJD) and KIR with KEAP1 (PDB ID: 3WDZ), however the structure of SQSTM1-UBA domain in complex with ubiquitin is unknown. These complexes clearly show that the sites of PR-ubiquitination (S361, S365, S366) were in very close proximity of KIR domain but not near the LIR and UBA domains. We further added ubiquitin on S361 of SQSTM1 and predicted the complexes. As expected, the binding of S361 ubiquitinated SQSTM1 reduced binding to KEAP1,

this largely due to the steric exclusion of KIR from the KEAP1 pocket due to presence of ubiquitin (Figure 1).

### PR-Ub of SQSTM1 inhibited recruitment of KEAP1 to intracellular bacteria

Previous reports showed that ~10% Legionella containing vacuoles were positive for SQSTM1 in the first 2–3 h post infection (Omotade and Roy, 2020). To check if SQSTM1 was recruited to intracellular Legionella upon infection and whether this was affected by PR-Ub we checked the localization of WT and PR-Ub-deficient MYC-SQSTM1 2 h.p.i. We observed about 40% of infected A549 cells expressing MYC-SQSTM1 to have at least one intracellular bacterium which was positive for SQSTM1. The PR-Ub-deficient mutant of SQSTM1 (SQSTM1<sup>S361,S365,S366A</sup>) was also bound to intracellular bacteria in a similar manner (Figure 2A). This suggested that SQSTM1 was recruited to intracellular bacteria vacuoles in the early part of the infection cycle and this was independent of its PR-Ub. Similarly, previous studies in *Salmonella* have shown the presence of SQSTM1 and KEAP1 at intracellular bacterial vacuoles. Phosphorylation of SQSTM1 at S351 was important for SQSTM1-KEAP1 interaction and recruitment of KEAP1 to SQSTM1-positive bacterial vacuoles [6]. To test whether endogenous KEAP1 was recruited to intracellular Legionella, A549 cells were depleted of endogenous SQSTM1 by treatment with SQSTM1 siRNA for 48 h, followed by reconstitution with WT and PR-Ub-deficient MYC-SQSTM1. Cells were then infected with WT or  $\Delta S$  Legionella for 2 h followed by immunofluorescence analysis of infected cells. This experiment showed that PR-Ub of SQSTM1 prevented KEAP1 recruitment to intracellular bacteria. KEAP1 was recruited to bacteria in  $\Delta S$  Legionella infection and in cells expressing PR-Ub-deficient SQSTM1 (Figure 2B). A549 cells depleted of endogenous SQSTM1 followed by reconstitution with MYC-tagged WT or PR-Ub-deficient SQSTM1 were infected with WT Legionella. Lysates were collected from infected cells at different time points post infection and analyzed for phosphorylation of SQSTM1 at S351. PR-ubiquitination did not affect the recognition of phosphorylated SQSTM1 with the phospho (S351) SQSTM1 antibody. Legionella infection triggered phosphorylation of SQSTM1 at S351; the amount of p-S351-SQSTM1 increased with time and was unaffected by PR-Ub. The SQSTM1-KEAP1 interaction was reduced by PR-Ub at 1 h.p.i. and at 2 h.p.i.

incubated with gst-tagged KEAP1 or GST alone in a GST affinity-isolation assay, followed by western blotting with GST and SQSTM1 antibodies. This experiment was repeated three times with similar results. Error bars, standard deviation, \* 0.05 > p ≥ 0.01, \*\* 0.01 > p ≥ 0.001. (E) GST-SQSTM1 (amino acids 321–400) of SQSTM1 purified from *E. coli*, was pr-ubiquitinated it in an *in vitro* reaction or left unmodified and incubated it with cell lysate from HEK293T cells infected with WT legionella in a GST affinity-isolation assay, followed by mass spectrometric identification of interactors. (F) A549 cells were transfected with MYC-SQSTM1 and infected with indicated legionella strains for 2 h, followed by immunoprecipitation of MYC-SQSTM1 and western blotting with LC3, ub, KEAP1, and MYC antibodies. This experiment was repeated three times with similar results. Error bars: standard deviation, \* 0.05 > p ≥ 0.01, \*\* 0.01 > p ≥ 0.001. (G) A549 cells were transfected with myc-tagged WT SQSTM1 or SQSTM1<sup>S361,S365,S366A</sup> and infected with indicated legionella strains for 2 h, followed by immunoprecipitation of MYC-SQSTM1 and western blotting with KEAP1, and SQSTM1 antibodies. This experiment was repeated three times with similar results. Error bars: standard deviation, \* 0.05 > p ≥ 0.01, \*\* 0.01 > p ≥ 0.001. (H) AlphaFold prediction of the complex formed between the SQSTM1 peptide (amino acids 321–400) and LC3 or KEAP1. (n.l.: not infected; WT: wild-type Legionella;  $\Delta S$ :  $\Delta$ Side Legionella;  $\Delta D$ :  $\Delta$ DupA/B legionella.) [change labels to "SQSTM1"].

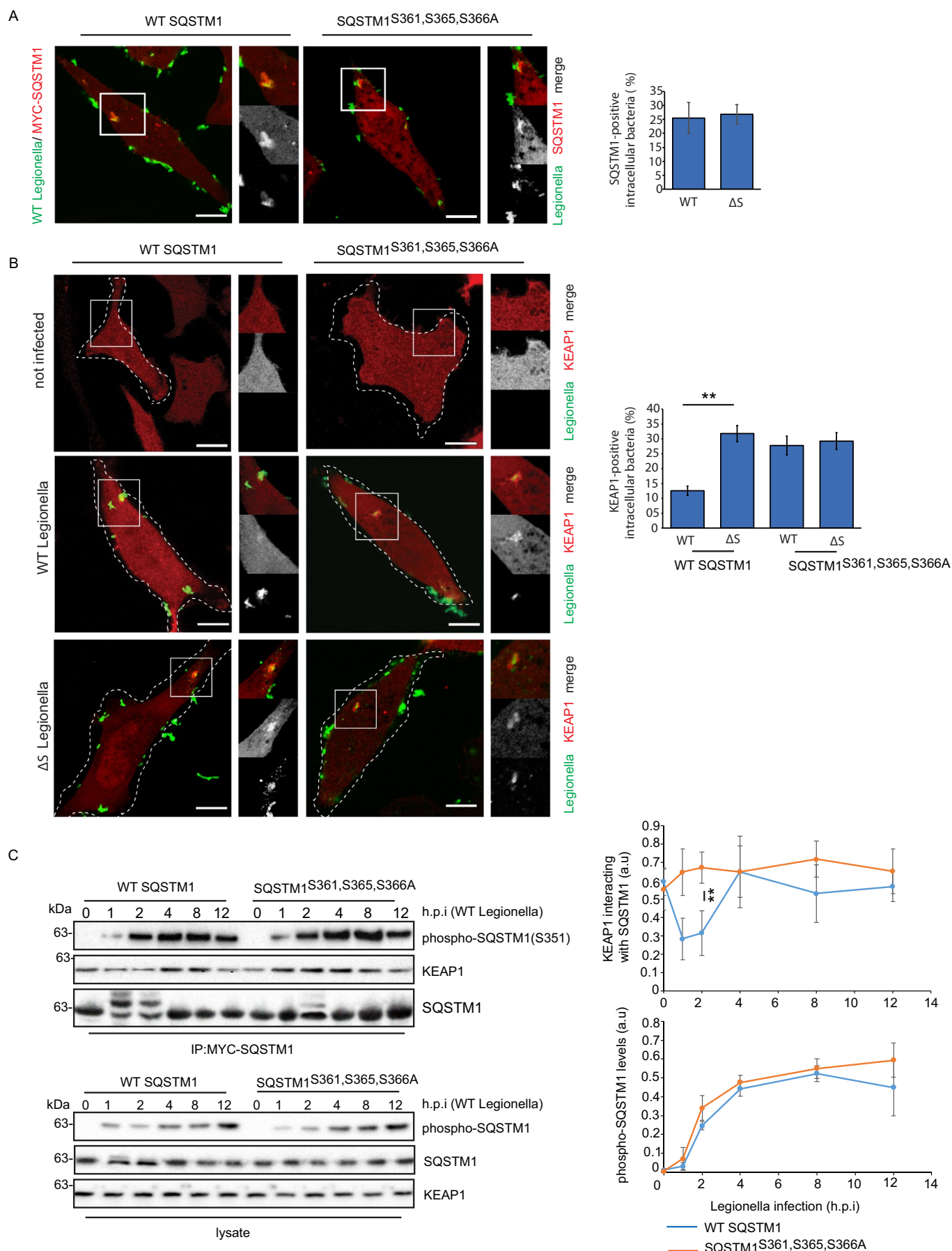


**Figure 2.** PR-Ub of SQSTM1 blocked KEAP1 recruitment to intracellular bacteria. (A) A549 cells expressing myc-tagged wild type or PR-Ub-deficient SQSTM1 (SQSTM1<sup>S361,S365,S366A</sup>) were infected with WT legionella followed by fixation and immunostaining at 2 h.p.i. To visualize recruitment of MYC-SQSTM1 to bacteria. 60

At later time-points, PR-Ub-modified SQSTM1 was not detected and the SQSTM1-KEAP1 interaction was similar to that in uninfected cells (Figure 2C).

### **The interaction between KEAP1 and NFE2L2 was modulated by the PR-Ub of SQSTM1**

To see if the reduced interaction between SQSTM1 and KEAP1 regulated the interaction between KEAP1 and NFE2L2, we immunoprecipitated KEAP1 from cells expressing WT SdeA or its catalytic mutant SdeA(EA/AA). WT SdeA expressing cells showed higher interaction between KEAP1 and NFE2L2 compared to cells expressing SdeA(EA/AA) or those with the control vector (Figure S1D).

Next, we tested how NFE2L2 levels are regulated during the infection time course by using A549 cells depleted of endogenous SQSTM1 by siRNA treatment and infected with WT Legionella, lysed at different time-points post infection and analyzed by western blotting to detect NFE2L2 levels. NFE2L2 levels were slightly higher in control siRNA treated cells compared to cells treated with SQSTM1 siRNA. NFE2L2 levels increased with the progress of the infection suggesting an activation of NFE2L2 signaling at later stages of infection (4–12 h.p.i.). Reconstitution of SQSTM1 depleted cells with WT or PR-Ub-deficient SQSTM1 followed by bacterial infection showed a dependence of NFE2L2 levels on PR-Ub of SQSTM1 at 4 h.p.i. and 6 h.p.i. At these time-points cells expressing the PR-Ub-deficient SQSTM1 had higher levels of NFE2L2 than those with WT SQSTM1. This is consistent with previous findings that upon PR-Ub, SQSTM1 did not bind to KEAP1 (Figure 1D–G). This caused KEAP1 to interact with NFE2L2 and cause its ubiquitination and proteasomal degradation (Figure 3A). A549 cells depleted of endogenous KEAP1 with siRNA, infected with either WT or  $\Delta$ S Legionella had higher NFE2L2 levels throughout the time course of infection (Figure 3B). Cells treated with the proteasomal inhibitor MG132 during infection caused stabilization of NFE2L2 at 4 and 6 h.p.i. Blocking the neddylation of CUL (cullin) RING ligases using MLN4924 also rescued the degradation of NFE2L2 during infection (Figure 3C).

SQSTM1 depleted cells were co-transfected with WT or PR-Ub-deficient SQSTM1 and MYC-NFE2L2 followed by infection with WT or  $\Delta$ S Legionella for 6 h. NFE2L2 was enriched from cell lysates on MYC resin and its ubiquitination was assayed by western blotting with anti-ubiquitin antibody. A greater amount of ubiquitinated NFE2L2 was observed in WT Legionella infected cells compared to uninfected or  $\Delta$ S infected cells. This difference of NFE2L2 ubiquitination was absent in cells expressing PR-Ub-deficient

SQSTM1 highlighting the importance of SQSTM1 PR-Ub in the regulation of NFE2L2 ubiquitination and degradation (Figure 3D). Further, lysates from infected cells were incubated with Tandem Ubiquitin Binding Entities 2 (TUBE2) agarose resin to enrich polyubiquitinated proteins from the cell. More ubiquitinated NFE2L2 was present in WT Legionella infection compared to uninfected and  $\Delta$ S Legionella infected cells. Treatment with MLN4924 led to a significant loss of NFE2L2 ubiquitination and an increase in NFE2L2 protein levels in all the experimental sets (Figure 3E). These experiments proved that both SQSTM1 and KEAP1 were important in regulating NFE2L2 levels through its KEAP1 mediated ubiquitination and proteasomal degradation during the course of Legionella infection.

### **NFE2L2-mediated antioxidant responses were dependent on PR-Ub of SQSTM1**

MYC-NFE2L2 expressing A549 cells were infected with different strains for 6 h followed by fractionation of lysates into nuclear and cytosolic fractions. WT and  $\Delta$ D Legionella infected cells had significantly lower levels of MYC-NFE2L2 in nuclear fractions suggesting lower NFE2L2-dependent transcription (Figure S1E). To assay NFE2L2-dependent transcription from antioxidant response elements we used A549 cells expressing the reporter ARE-Luciferase. These cells were depleted of endogenous SQSTM1 by treatment with SQSTM1 siRNA followed by reconstitution with WT or PR-Ub-deficient SQSTM1, infected with WT Legionella and assayed for ARE-luciferase activity at different time points of infection. Cells expressing WT SQSTM1 had lower NFE2L2-dependent ARE transcription at 6 and 8 h.p.i., when compared to cells expressing mutant SQSTM1 (Figure 3D). At 6 h.p.i. WT Legionella infected cells had lower NFE2L2-dependent transcription than  $\Delta$ S Legionella infected cells (Figure S1F).

### **NFE2L2-dependent gene expression was downregulated upon acute legionella infection**

A549 cells were infected with WT or  $\Delta$ S Legionella for 6 h followed by extraction of total mRNA. Next generation RNA sequencing was performed using the Illumina platform to check differential expression of genes. Expression of several known NFE2L2 target genes including HMOX1 (heme oxygenase 1), MT1X (metallothionein 1X), TXNRD1 (thioredoxin reductase 1), SOD2 (superoxide dismutase 2), CAT (catalase), SQSTM1 (sequestosome 1), SLC48A1 (solute carrier family 48 member 1), and NQO1 (NAD (P)H quinone dehydrogenase 1)

---

cells were analyzed in FIJI manually to count the number of SQSTM1-positive bacteria and numbers were plotted in MS excel. Scale bar: 10  $\mu$ m. (B) A549 cells expressing myc-tagged wild type or PR-Ub deficient SQSTM1 were infected with WT or  $\Delta$ S legionella followed by fixation and immunostaining with KEAP1 at 2 h.p.i., legionella antibodies to visualize recruitment of KEAP1 to bacteria. 60 cells were analyzed in FIJI manually to count the number of KEAP1-positive bacteria and the numbers were plotted in MS excel. Error bars, standard deviation, \*\* 0.01 > p  $\geq$  0.001. Scale bar: 10  $\mu$ m. (C) A549 cells expressing myc-tagged wild-type or PR-Ub-deficient SQSTM1 were infected with WT legionella and lysed at indicated time-points followed by immunoprecipitation of SQSTM1-MYC and western blotting with antibodies against SQSTM1, p(S351)-SQSTM1, and KEAP1. Graphs indicate quantitation of band intensities of 3 immunoblots taken from 3 independent experiments. Error bars indicate standard deviation, \*\* 0.01 > p  $\geq$  0.001.

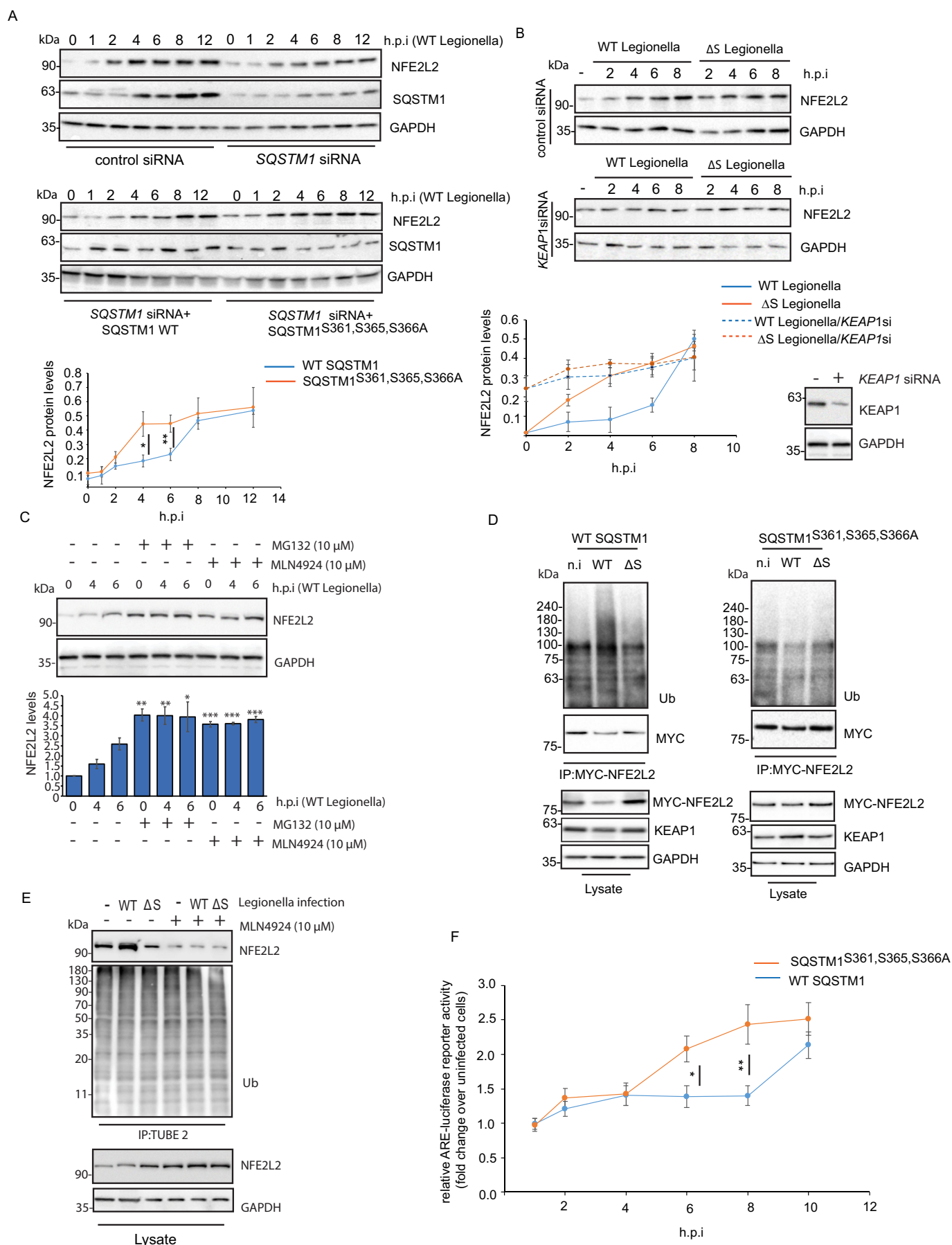


**Figure 3.** PR-Ub of SQSTM1 induced NFE2L2 ubiquitination and degradation. (A) A549 cells were treated with SQSTM1 siRNA for 48 h followed by reconstitution with wild type or PR-Ub-deficient SQSTM1 (SQSTM1<sup>S361,S365,S366A</sup>) for 24 h. these are then infected with WT legionella and lysed at indicated time-points. Lysates are blotted



were higher in  $\Delta S$  Legionella infection compared to cells infected with WT Legionella (Figure 4A and S2A). Gene Ontology (GO) analysis of differentially expressed genes using the online server MetaScape identified oxidative stress response, peroxisome and pyruvate metabolism and TCA cycle to be the pathways upregulated in  $\Delta S$  Legionella infection when compared to infection with the wild-type bacteria. WT Legionella infection led to upregulation of genes related to other GO classes like VEGFR signaling, DNA damage response and cytokine signaling (Figure S2B-D). NFE2L2/NRF2 mediated regulation of gene expression was identified as the most transcriptionally upregulated pathway in  $\Delta S$  Legionella infection. Transcriptional pathways regulated by NFkB/NF- $\kappa$ B (nuclear factor kappa B), TP53/p53 (tumor protein p53) and HIF1A/HIF-1 $\alpha$  (hypoxia inducible factor 1 subunit alpha) were upregulated in WT Legionella infection (Figure S2E and S2F).

Next, we infected A549 cells with WT or  $\Delta S$  Legionella in the presence of the NFE2L2 activator tBHQ (tertiary butylhydroquinone) or the NFE2L2 inhibitor ML385 for 6 h followed by extraction of mRNA and quantitative PCR to measure the differential expression of NFE2L2 target genes. Similar to our RNA sequencing data, WT Legionella infected cells had lower levels of NFE2L2 target genes including HMOX1, TXNRD1, SOD2, NQO1 and SQSTM1 when compared to cells infected with  $\Delta S$  Legionella. Upon treatment with tBHQ, WT Legionella infected cells (where NFE2L2 was degraded by KEAP1) showed a slight to moderate increase in expression of NFE2L2 targets, while  $\Delta S$  Legionella infected cells showed a significant increase in expression of NFE2L2 target genes. Conversely, treatment with ML385 had almost no effect in expression levels of NFE2L2 targets in WT Legionella infected cells as NFE2L2 mediated gene expression is already blocked through PR-Ub-mediated regulation of the SQSTM1-KEAP1-NFE2L2 signaling pathway.  $\Delta S$  Legionella infected cells treated with ML385 showed a significant reduction in NFE2L2-dependent gene expression (Figure 4B). We also tested protein levels of NFE2L2 regulated antioxidants SOD2, HMOX1/HO-1, and NQO1 in Legionella infected cells. Expression of these antioxidants were lower in WT Legionella infection when compared to  $\Delta S$  infection. Expression of the PR-Ub-deficient mutant of SQSTM1 (SQSTM1<sup>S361,365,366A</sup>) in SQSTM1 depleted cells abolished this difference in antioxidant levels (Figure 4C). Collectively these experiments indicated that in WT Legionella infection, NFE2L2-dependent expression of antioxidants is blocked through PR-Ub of SQSTM1; KEAP1

can interact with NFE2L2 causing its ubiquitination and proteasomal degradation. In absence of PR-Ub (as in  $\Delta S$  Legionella infection), phosphorylated SQSTM1 (p-S351-SQSTM1) binds to KEAP1, leading to stabilization of NFE2L2 and expression of its downstream targets.

### Cellular ROS levels were regulated in a PR-Ub-dependent manner

Since PR-Ub of SQSTM1 regulated antioxidant levels, we decided to check the levels of total cellular ROS at different time-points of infection. For this Legionella infected cells were loaded with the oxidative stress sensitive fluorogenic probe CellROX green for 30 min, fixed with paraformaldehyde and imaged by high content fluorescence microscopy. WT Legionella infection led to higher ROS levels at 6 and 8 h.p.i. when compared to infection with the  $\Delta S$  strain. At 10 h.p.i. ROS levels were similar between the WT and  $\Delta S$  infected cells (Figure 4D). Treatment of infected cells with tBHQ and ML385 reduced and increased ROS levels respectively underlining the dependence of cellular ROS in infected cells on the NFE2L2 pathway (Figure 4E).

A549 cells were transfected with a mitochondria targeted redox-sensitive GFP probe (mito-roGFP) which is a ratiometric reporter of oxidative stress in live cells. Similar to the total ROS measurements, mitochondrial ROS was higher in WT Legionella infection compared to the  $\Delta S$  bacteria at 8 h.p.i (Figure 4F). Infection of cells containing a cytosolic variant of redox GFP also showed similar results (Figure 4G).

### PR-Ub of SQSTM1 remodelled the proteome in a NFE2L2-dependent manner.

We infected A549 cells with WT or  $\Delta S$  Legionella in the presence of tBHQ or ML385 for 8 h followed by protein extraction and analysis of the whole cell proteome and phosphoproteome by mass spectrometry to identify the NFE2L2-dependent changes in the proteome (Figure 5A). In uninfected cells treatment with tBHQ for 8 h led to the significant increase in expression of known NFE2L2-dependent genes including SQSTM1, antioxidants (NQO1, TXNRD1, GPX2, SOD2, CAT), and glycolysis enzymes (HK1, G6PD, TALDO1). Treatment with ML385 led to an increase in enzymes related to fatty acid metabolism (ACOX1, DGAT1, HACD2, ACADS, ACSM5, SCD, SELENOI), proteins related to mitochondrial respiration (MT-CO3, MT-CO1, SDHD,

---

with SQSTM1, NFE2L2, GAPDH antibodies. Graphs indicate quantitation of band intensities of 3 immunoblots taken from 3 independent experiments. Error bars indicate standard deviation. (B) A549 cells were treated with KEAP1 siRNA for 48 h followed by infection with WT or  $\Delta S$  legionella and lysed at indicated time-points. Lysates are blotted with NFE2L2, and GAPDH antibodies. Graphs indicate quantitation of band intensities of 3 immunoblots taken from 3 independent experiments. Error bars indicate standard deviation. (C) Cells infected with WT legionella were lysed at 4 and 6 h.p.i. 10  $\mu$ M MG132 or MLN4924 was added for 2 h prior to lysis. Lysates were immunoblotted with NFE2L2 and GAPDH levels. This experiment was repeated three times with similar results. Error bars indicate standard deviation, \* 0.05 >  $p$   $\geq$  0.01, \*\* 0.01 >  $p$   $\geq$  0.001, \*\*\*  $p$  < 0.001. (D) A549 cells expressing MYC-NFE2L2 and SQSTM1 (wild type or PR-Ub deficient) were infected with WT or  $\Delta S$  legionella for 6 h, NFE2L2 ubiquitination was probed by immunoprecipitating NFE2L2-MYC and western blotting with ub. This experiment was repeated three times with similar results. (E) A549 cells were infected with WT or  $\Delta S$  legionella for 6 h in presence or absence of 10  $\mu$ M MLN4924. 10  $\mu$ M MG132 was added to all sets for 2 h prior to lysis. Polyubiquitinated proteins were enriched from lysates using TUBE2 resin followed by western blotting to assess levels of ubiquitinated NFE2L2. This experiment was repeated three times with similar results. (F) A549 cells cotransfected with are (NFE2L2 promoter)-luciferase reporter construct and wild-type or PR-Ub-deficient SQSTM1 were infected with legionella for indicated times followed by measurement of luciferase reporter activity. Graph represents are-luciferase activity expressed as the fold change from uninfected cells. Error bars indicate standard deviation, \* 0.05 >  $p$   $\geq$  0.01, \*\* 0.01 >  $p$   $\geq$  0.001.

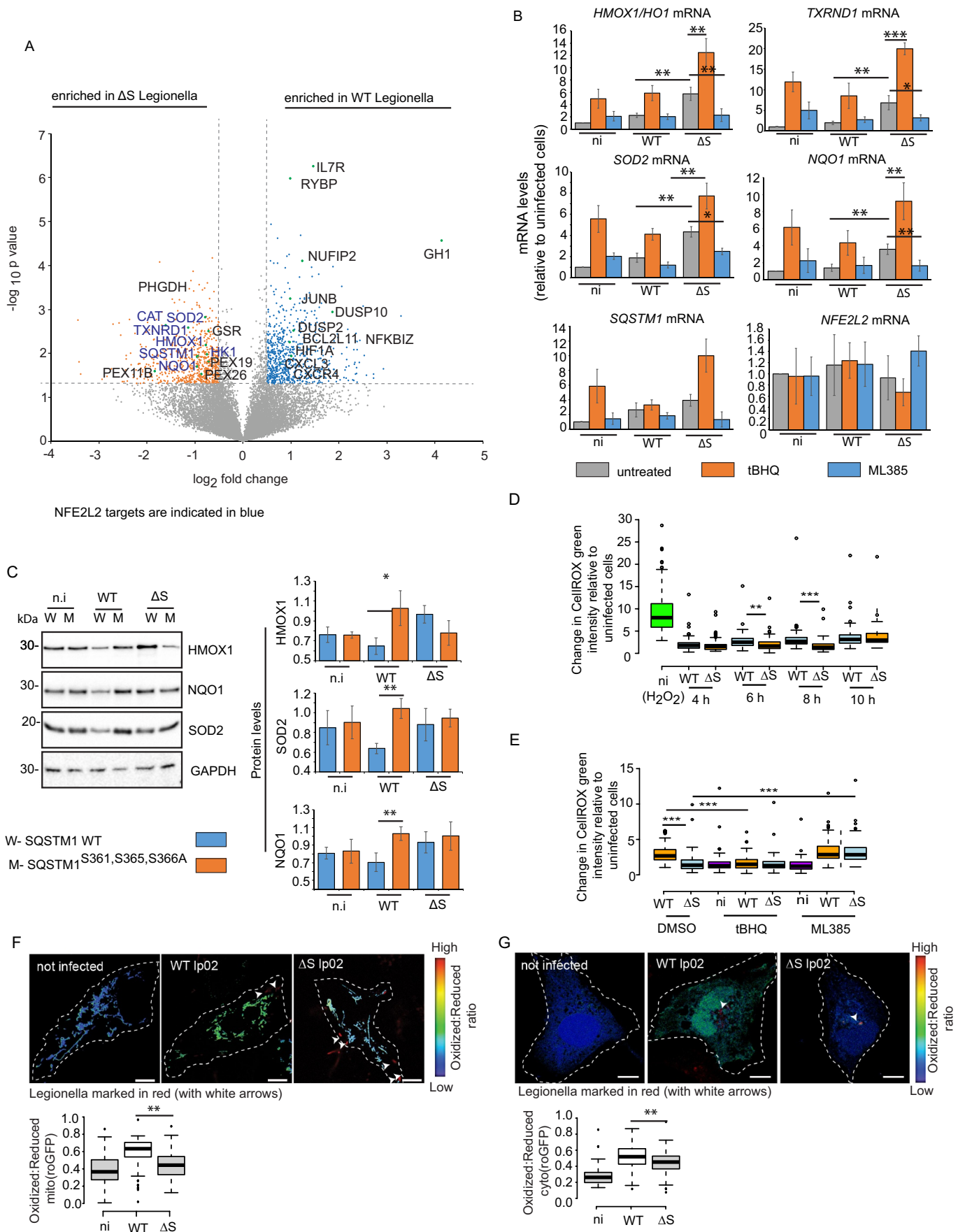


**Figure 4.** PR-Ub of SQSTM1 regulated NFE2L2-dependent gene expression. (A) Differential expression of genes between WT and  $\Delta S$  legionella infection. (B) RT-PCR to measure expression of NFE2L2 targets in A549 cells infected with WT or  $\Delta S$  legionella for 6 h in presence of 10  $\mu$ M tBHQ or ML385. (C) A549 cells expressing wild-type or PR-Ub-deficient SQSTM1 were infected with WT or  $\Delta S$  legionella for 6 h followed by western blotting of lysates with indicated

ATP6, COX7C), and proteins related to steroid biosynthesis (EBP, HMGCR, CYP24A1, SDHC, APOC3, MSMO1, CYP5A1) (Figure 5B,C). This indicated a NFE2L2-dependent remodeling of the proteome in A549 cells. Upon infection of cells with WT Legionella, both tBHQ and ML385 did not have any significant impact on the change in NFE2L2-dependent antioxidants which was consistent with the high ROS levels observed in WT Legionella infection. Though these cells were less responsive to NFE2L2 activation, other pathways related to metabolic changes and mitochondrial respiration were altered. tBHQ treatment increased levels of mitochondrial proteins (COX7C, NDUFB8, NDUFC1, ATP5MG, ATP5MF, UQCRCQ, NIPSNAP1), enzymes involved in glucuronate metabolism (UGT1A1, UGT2A3, UGT2B7, CYP1B1, CYP3A5) (Figure S3A-D). Infection of cells with  $\Delta S$  Legionella led to an increase in NFE2L2-dependent antioxidants and metabolic enzymes. Blocking NFE2L2-dependent gene expression with ML385 led to increased expression of peroxisomal genes (PEX2, PEX13, PMP34, MPV17, HSD17B), and other genes related to detoxification of ROS (TXN2, TXNDC1, TMX4, TMX1, PRDX3) (Figure 5D,E and S3E). Analysis of the transcription regulatory networks regulated in a tBHQ dependent manner in uninfected, WT and  $\Delta S$  Legionella infection utilizing the online tool TRRUST (transcriptional regulatory relationships unravelled by sentence-based text-mining, [29]) identified NFE2L2 to be within the top hits altered by tBHQ treatment in uninfected and  $\Delta S$  Legionella infected cells; WT Legionella infection did not show induction of NFE2L2-dependent genes (Figure S4A-C). Phosphoproteome analysis of Legionella infected cells treated similarly as shown in Figure 5A led to identification of 1525 phosphosites including serine, threonine and tyrosine residues (Figure S5A). 67 proteins and 164 proteins were differentially phosphorylated in WT and  $\Delta S$  Legionella infection respectively. GO analysis of proteins differentially regulated by phosphorylation in WT Legionella infection led to enrichment of terms related to cellular metabolism (Figure S5B and S5C). Proteins differentially regulated by phosphorylation in  $\Delta S$  Legionella infection included those related to RNA binding, transcription and cellular response to stress (Figure S5D).

### **PR-Ub-mediated remodelling of oxidative metabolism favored bacterial replication in host cells**

To check how the redox modulation of the transcriptome and proteome during infection affects bacterial proliferation in the host cell we performed an intracellular replication assay of Legionella under conditions of oxidative stress induced by increasing concentration of H<sub>2</sub>O<sub>2</sub>. We found that replication

of WT bacteria was unaffected by a low concentration of H<sub>2</sub>O<sub>2</sub> (0.1  $\mu$ M). However, the same concentration of H<sub>2</sub>O<sub>2</sub> was enough to cause a significant reduction in the intracellular replication of  $\Delta S$  Legionella. Higher concentrations of H<sub>2</sub>O<sub>2</sub> (1  $\mu$ M and 5  $\mu$ M) reduced bacterial replication of both WT and  $\Delta S$  Legionella (Figure 5F). 5  $\mu$ M H<sub>2</sub>O<sub>2</sub> also reduced the viability of A549 cells in an MTT assay (Figure S5E). Depletion of either NFE2L2 or KEAP1 in host cells reduced the intracellular replication of WT Legionella in presence of 0.1  $\mu$ M H<sub>2</sub>O<sub>2</sub> (Figure 5G). To check whether PR-Ub of SQSTM1 altered bacterial replication in the host cell we depleted endogenous SQSTM1 with siRNA for 48 h followed by reconstitution with WT or ser mut SQSTM1 for 24 h followed by infection with WT Legionella. Knockdown of SQSTM1 enhanced intracellular replication of bacteria, suggesting that SQSTM1 May be a part of the host defense which combats bacterial proliferation. Reconstitution with WT SQSTM1 resulted in Legionella replication which resembled that in control siRNA treated cells; whereas, reconstitution with the PR-Ub-deficient mutant reduced intracellular replication of bacteria. This experiment suggested that PR-Ub of SQSTM1 is important for bacterial replication in the host cell through the KEAP1-NFE2L2 pathway but SQSTM1 May also be a part of the host defense to stop bacterial replication (Figure S5F).

Collectively, this study shows how serine ubiquitination of SQSTM1 prevents NFE2L2 activation in the first few hours of infection. By 4 h.p.i., PR-Ub-SQSTM1 levels drop significantly, allowing transcriptional activation of NFE2L2 target genes at a later stage of infection (Figure 5H).

## **Discussion**

This study shows how Legionella utilizes serine ubiquitination to fine-tune redox metabolism of the infected cell through the regulation of the SQSTM1-KEAP1-NFE2L2 signaling axis. Upon PR-Ub, SQSTM1 is sterically prevented in binding to KEAP1, which is then available to interact with NFE2L2, causing its ubiquitination and proteasomal degradation. This mechanism prevents the premature activation of the NFE2L2-dependent redox response in the early stage of infection. The activity of DUPs causes the levels of PR-Ub-SQSTM1 to drop and completely disappear by 4 h.p.i. [22]; removing the SQSTM1-KEAP1 mediated inhibition on NFE2L2 activation, providing a temporal regulation of the transcription of NFE2L2 target genes.

In parallel, Legionella infection triggers the phosphorylation of SQSTM1 at S351 within the first 1 h of infection. In absence of PR-Ub (as in  $\Delta S$  Legionella), p-S351-SQSTM1 competes with NFE2L2 for binding to KEAP1. As a result,

---

antibodies. Graphs represent band intensities from 3 experiments, error bars indicate standard deviation. \*0.05>p ≥ 0.01, \*\* 0.01>p ≥ 0.001. (D) Total ROS measured in infected cells at indicated time-points by oxidative stress indicator CellROX green. Data represents 100 cells taken from 3 independent experiments. \*\*\* 0.001>p, \*\* 0.01>p ≥ 0.001. (E) CellROX green measurements at 8 h.p.i in cells infected with legionella in presence of 10  $\mu$ M tBHQ or ML385. Data represents 100 cells taken from 3 independent experiments. \*\*\* 0.001>p. (F) Mitochondrial roGFP measurements in legionella infected cells 8 h.p.i. Data represents 60 cells taken from 3 independent experiments. \*\* 0.01>p ≥ 0.001. Scale bar: 10  $\mu$ m. (G) Cytosolic roGFP measurements in legionella-infected cells 8 h.p.i. Data represent 60 cells taken from 3 independent experiments \*\* 0.01>p ≥ 0.001. Scale bar: 10  $\mu$ m.

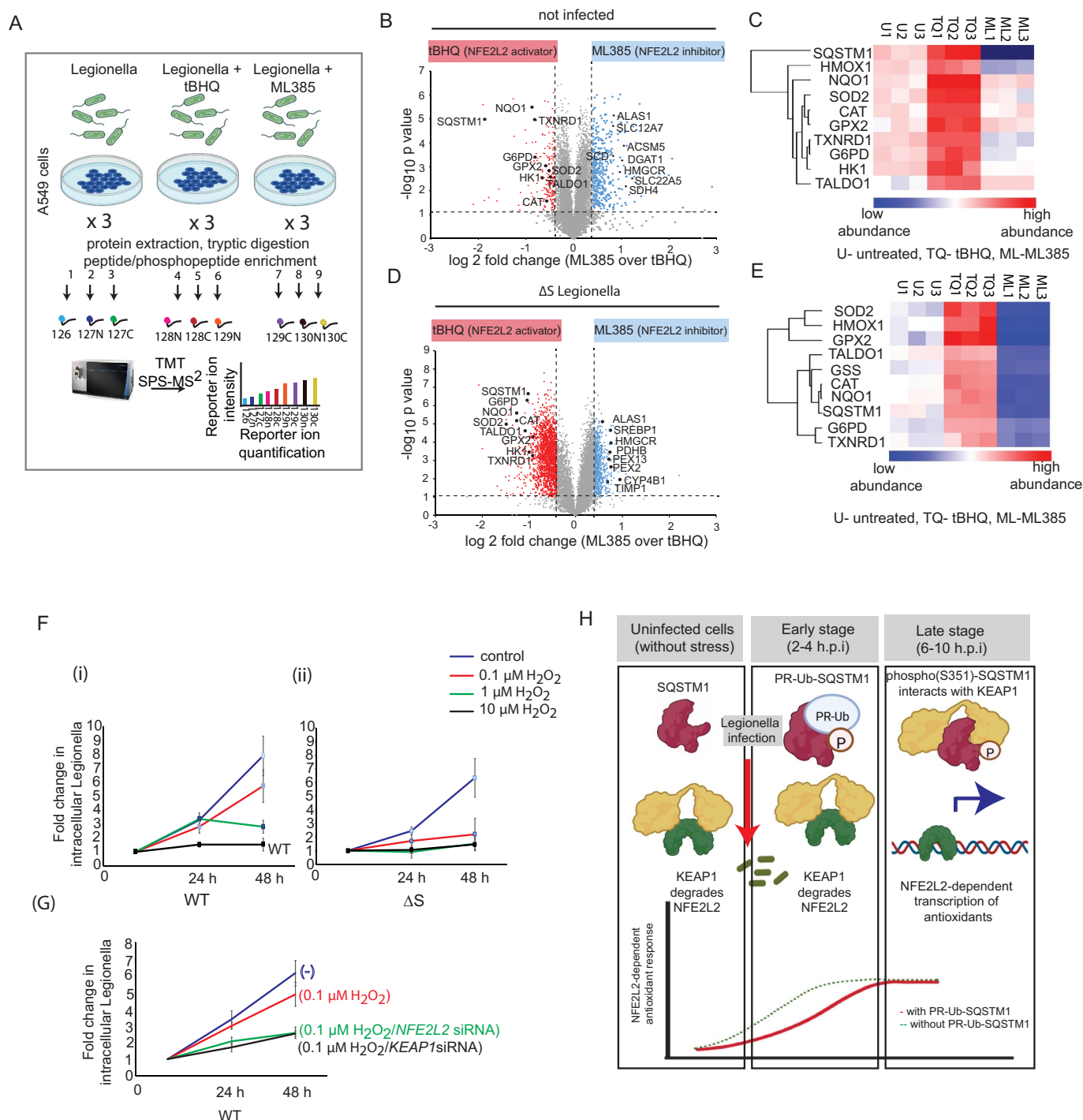


**Figure 5.** Legionella infection caused remodeling of the host proteome in a NFE2L2-dependent manner. (A) Schematic of experimental strategy. (B) Volcano plot showing changes in the proteome of A549 cells when treated with 10  $\mu$ M tBHQ or 10  $\mu$ M ML385 for 8 h. (C) Levels of NFE2L2-dependent genes in the experiment indicated in panel B. (D) Volcano plot showing changes in the proteome of A549 cells infected with  $\Delta$ S legionella in presence of 10  $\mu$ M tBHQ or 10  $\mu$ M ML385 for 8 h. (E) Heatmap showing levels of NFE2L2 pathway proteins in the experiment indicated in panel D. (F) A549 cells were infected with WT or  $\Delta$ S legionella for 12 h, 24 h or 48 h in presence of  $H_2O_2$  followed by estimation of intracellular bacterial load measured by a bacterial replication assay. (G) A549 cells depleted of endogenous KEAP1 or NFE2L2 were infected with legionella for 12 h, 24 h or 48 h in presence of  $H_2O_2$  followed by estimation of intracellular bacterial load measured by a bacterial replication assay. (H) Summary showing effect of PR-Ub on the SQSTM1-KEAP1-NFE2L2 pathway. (transcriptional networks regulated by tBHQ which are shared between uninfected and  $\Delta$ S legionella infection are marked in red).

NFE2L2 is stabilized and transcription of NFE2L2 targets are activated at an early phase of infection. Therefore, PR-Ub does not interfere with the phosphorylation of SQSTM1 but delays the activation of NFE2L2 to a later stage of infection.

*Legionella pneumophila* has several effectors which block autophagy in the host cell. The most prominent of these bacterial proteins is RavZ which delipidates Atg8-family proteins, blocking the formation of autophagosomes. Therefore,

Legionella infected cells can be considered as an autophagy-deficient system where there may be buildup of ubiquitinated autophagic cargo (like ubiquitinated bacteria, defunct mitochondria, or protein aggregates) which can bind SQSTM1, form SQSTM1 oligomers and lead to activation of the SQSTM1-KEAP1-NFE2L2 signaling cascade. In the absence of a functional autophagy-lysosomal system, phospho-(S351)-SQSTM1 remains elevated throughout the infection time-course (measured up to 12 h.p.i.). Though SQSTM1-positive autophagosomes are not formed during infection, our studies and others have reported the recruitment of SQSTM1 to ubiquitinated Legionella [30]. From the immunofluorescence analysis, we infer that serine ubiquitination of SQSTM1 does not affect its recruitment to the bacterial phagosome in the early phase of infection but prevented the recruitment of KEAP1 to the bacterial phagosomes. In absence of PR-Ub, the p-S351-SQSTM1-KEAP1 interaction on ubiquitinated bacterial phagosomes lead to the stabilization and nuclear translocation of NFE2L2.

NFE2L2 is an important signaling hub which regulates several aspects of metabolism. Our results indicate that NFE2L2 ubiquitination has an impact on transcription of ROS detoxification enzymes (like TXNRD1, NQO1, SOD2, etc) and their regulation on the cellular ROS levels at different time-points of infection. It is also important to consider that NFE2L2 target genes include several metabolic enzymes including those involved in glycolysis and pyruvate metabolism. These include HK1 (hexokinase 1), TALDO1 (transaldolase 1), G6PD1 (glucose-6-phosphate dehydrogenase), PGD (phosphogluconate dehydrogenase). Our RNAseq data showed that these NFE2L2 target genes were also downregulated in WT Legionella infection suggesting a differential regulation of carbon flux through glycolysis and the pentose phosphate pathway. Pathway analysis to compare gene expression differences between WT and  $\Delta$ S Legionella infection identified carbon metabolism, carbohydrate metabolism, pyruvate metabolism, and TCA cycle to be within the top 20 hits suggesting a serine ubiquitin dependent remodeling of metabolism, which may be partially dependent on NFE2L2. Previous studies on macrophages infected by Legionella have reported changes in mitochondrial respiration and glycolysis induced by bacterial effectors. A shift to glycolytic (Warburg-like) metabolism at a later phase of infection promotes proliferation of Legionella [31]. Our studies suggest that NFE2L2-dependent regulation of gene expression may have an important role in determining the metabolic switch to glycolysis. NFE2L2 signaling is also linked with inflammation; cross-talk of NFE2L2 signaling with the NF $\kappa$ B pathway has been characterized in several cases [32,33]. The NFE2L2 target gene *HMOX1* encodes heme oxygenase 1 which modulates intracellular iron metabolism and negatively regulates inflammation [34]. Whether and how iron metabolism and inflammation are regulated by serine ubiquitination will be further studied in the future.

It is interesting to contemplate how the serine ubiquitination mediated regulation of the redox response affects intracellular Legionella. The intracellular replication assay suggests that WT Legionella can survive and proliferate in cells treated with the oxidative stressor (1  $\mu$ M H<sub>2</sub>O<sub>2</sub>), while in the case of

$\Delta$ S Legionella, the intracellular replication is significantly compromised. The NFE2L2-dependent remodeling of gene expression contributes to the better tolerance of WT bacteria to oxidative stress as siRNA mediated depletion of NFE2L2 and KEAP1 reduced bacterial replication significantly. The better tolerance to oxidative stress may be due to differential regulation of metabolic pathways that affect nutrient availability to the bacteria. It may also be affected by differences in activation of cell death pathways between WT and  $\Delta$ S Legionella infection. Studies on UPEC have demonstrated how NFE2L2-dependent transcription of *RAB27B* helps in expulsion of bacteria from urothelial cells at a late stage of infection [35]. It may be possible to envision circumstances where the optimal timing of bacterial release from Legionella infected cells is influenced by PR-Ub-dependent NFE2L2 activation, which in turn would influence the intracellular load of bacteria at a given time.

## Materials and methods

### Plasmid construction

cDNA for human *SQSTM1* (NCBI reference number: NM\_003900.5) was cloned with an N-terminal MYC tag in pCMV3 vector (SinoBiological, CV011) and in pcDNA3-HA2-KEAP1 and pcDNA3-MYC3-NFE2L2 are gifts from Yue Xiong (Addgene 21,556 and 21,555); [36]. Matrix-roGFP and cyto-roGFP was a gift from Paul Schumacker (Addgene 49,437 and 49,435) [37]. pLminP\_Luc2P\_RE4 was a gift from Ramnik Xavier (Addgene 90,338), [38]. GST-tagged KEAP1 and ubiquitin were generated by cloning human cDNA sequences into pGEX6P1 (Sigma, GE28-9546-48). Point mutations in *SQSTM1* were introduced by standard site directed mutagenesis.

### Protein purification

GST-tagged DupA, KEAP1 and ubiquitin were purified from *E. coli* as previously described [22]. Briefly, BL21(DE3) competent cells (NEB, C2527H) were transformed with plasmids and grown in lysogeny broth at 37°C to an OD<sub>600</sub> of 0.6–0.8. Protein expression was induced by adding 0.5 mM isopropyl- $\beta$ -thiogalactopyranoside (IPTG; Sigma, I6758) overnight at 18°C. Lysates were incubated with glutathione sepharose resin (Sigma, GE17-0756-01) pre-equilibrated with lysis buffer (50 mM Tris-HCl, pH 7.5, 150 mM NaCl, 3 mM DTT), and nonspecific proteins were cleared by washing twice with wash buffer (50 mM Tris-HCl, pH 7.5, 300 mM NaCl, 3 mM DTT). Proteins were eluted in 50 mM Tris-HCl, pH 7.5, 150 mM NaCl, 15 mM glutathione (Sigma, GE17-0756-01) and exchanged into storage buffer (20 mM Tris-HCl, pH 7.5, 100 mM NaCl) before further use.

### Antibodies siRNA and other reagents

Human siRNA was used were as follows: *SQSTM1* siRNA (Santa Cruz Biotechnology, sc -29,679). *KEAP1* siRNA (Santa Cruz Biotechnology, sc -43,878), *NFE2L2* siRNA (Santa Cruz Biotechnology, sc -37,030).

We used the following antibodies and dilutions: SQSTM1 (BD Biosciences 610,832), KEAP1 (Cell Signaling Technology, 4678), NFE2L2 antibody (Santa Cruz biotechnology, sc -365,949), GAPDH (Cell Signaling Technology, 2118), MYC beads (Santa Cruz Biotechnology, sc -500,771), LC3 (Cell Signaling Technology, 2775), phospho-SQSTM1 (Cell Signaling Technology 95,697), ubiquitin (Cell Signaling Technology, 3933), HMOX1/HO1 (Santa Cruz Biotechnology, sc -136,960), NQO1 (abcam, ab34173), SOD2 (abcam, ab13533), GST resin (Pierce, ThermoFisher Scientific 16,101), Legionella antibody (abcam, ab20943). MLN4924 (Sigma Aldrich 505,477), MG132 (Sigma Aldrich, M7449).

### Immunoprecipitation and western blotting

Cells were lysed in 50 mM Tris-HCl, pH 7.5 containing 150 mM NaCl and 1% Triton X-100 (Fischer Scientific, PI85111). For the immunoprecipitation of MYC-SQSTM1 or MYC-NFE2L2, lysates containing 1 mg protein were incubated with MYC beads (Santa Cruz Biotechnology, sc -500,771) in immunoprecipitation buffer (50 mM Tris-HCl, pH 7.5, 150 mM NaCl, 0.5% Triton X-100), then washed (50 mM Tris-HCl, pH 7.5, 300 mM NaCl, 0.5% Triton X-100) and boiled with SDS sample buffer. For western blotting, 20- $\mu$ g samples were loaded onto 10% Tris-glycine gels and fractionated at 150 V for 1.5 h, followed by transfer to a PVDF membrane for 2 h at 300 mA and incubation with the antibodies listed above. For quantitation of western blots, chemiluminescence images were analyzed in the ImageLab software where intensity of bands was noted from at least 3 blots taken from 3 experiments.

### GST affinity-isolation assay

Cells were lysed (20 mM Tris-HCl, pH 7.5, 150 mM NaCl, 1% Triton X-100) and precleared by incubating with 30  $\mu$ L GST beads for 1 h to reduce nonspecific binding. We then added 1 mg of the precleared lysate to 5  $\mu$ g of GST-tagged protein and 20  $\mu$ L glutathione Sepharose resin, and incubated at 4°C for 2 h on a rotary shaker. The resin is then washed (20 mM Tris-HCl pH 7.5, 300 mM NaCl, 1% Triton X-100), boiled with SDS sample buffer and analyzed by western blot as described above.

### PR-Ub assay

MBP or His-tagged SQSTM1 were incubated at 37°C for 1 h with 25 mM of purified untagged ubiquitin, 1 mM NAD<sup>+</sup> (Sigma, N1511) and 1–2 mM SdeA in 50 mM Tris-HCl, pH 7.5, 50 mM NaCl. SdeA was purified in the lab as described previously [23]. The reaction mixture was processed as described for western blotting above, and probed with antibodies specific for ubiquitin and GST. PR-Ub-specific deubiquitination assays were performed by incubating PR-Ub proteins with 1  $\mu$ g of GST-DupA at 37°C for 1 h in a buffer containing 50 mM Tris-HCl, pH 7.5, 150 mM NaCl.

### Identification of PR-Ub sites

PR-Ub sites were identified by ETD-MS as previously described [26,39]. MBP-tagged SQSTM1 was modified by SdeA *in vitro* then denatured in 0.1 M Tris-HCl (pH 7.5) containing 8 M urea. The samples were washed three times in 200  $\mu$ L of the same buffer in a 30-kDa Amicon Ultra 0.5-mL centrifugal filter (Merck,UFC5030) to remove free ubiquitin. The eluted protein was washed twice in 50 mM ammonium bicarbonate, pH 7.5 before digestion using a 1:50 ratio of trypsin (Promega, V5111) the same buffer for 6 h. The peptides were desalted on a C18 column, followed by LC-MS/MS analysis. The spectra were collected and deconvoluted, and high-resolution ETD-MS/MS spectra were manually inspected to verify the sequence.

### Legionella infection

*Legionella pneumophila* strains were obtained from Dr. Zhao-Qing Luo (Purdue University) and were grown for 3 days on *N*-(2-acetamido)-2-amino-ethanesulfonic acid (ACES)-buffered charcoal (BCYE) extract agar (Sigma, A3495), at 37°C, followed by growth for 20 h in CYE medium (yeast extract [Sigma, Y1625] 10 g/L, charcoal 2 g/L, ferric pyrophosphate [Sigma, P6526], 0.25 g/L, ACES [Sigma, A9758] 10 g/L, cysteine [Thermo Scientific, A10435.30], 0.4 g/L). Bacterial cultures (OD<sub>600</sub> = 3.2–3.6) were used to infect HEK 293T, HeLa cells with a multiplicity of infection (MOI) of 10, and A549 cells with a MOI of 2. For 12 h infection experiments, we used a MOI of 1. HEK 293T and HeLa cells were transfected with CD32 16 h before infection to facilitate bacterial entry.

### Intracellular replication of Legionella

A549 cells growing in 35-mm dishes were infected with Legionella strains at a MOI of 1. The infection was allowed to proceed for 90 min in antibiotic-free medium before switching to medium containing gentamycin for 60 min to kill the remaining extracellular bacteria. The cells were then lysed in 0.4% saponin (Sigma 47,036) immediately or after 24 or 48 h to release intracellular bacteria. Lysates were spotted onto BCYE plates at 1:10 and 1:100 dilutions. The intracellular bacterial load was assessed by counting bacterial colonies formed after 48 h. The number of colony forming units (CFUs) was calculated using the formula  $\text{cfu/mL} = (\text{number of colonies} \times \text{dilution factor}) / \text{volume of sample plated (mL)}$ . The fold-increase in CFUs was calculated by normalizing the cfu at 24 or 48 h to that determined immediately after lysis.

### Confocal microscopy and image analysis

Confocal images were obtained using a Zeiss LSM780 microscope system fitted with a 63  $\times$  1.4 NA oil-immersion objective as well as argon and helium – neon ion lasers for the excitation of GFP (488 nm) and RFP (546 nm), respectively. Images were analyzed in FIJI to determine recruitment of proteins to bacteria. For statistical analysis, at least 50 cells were analyzed from 3 independent experiments.

For measurement of intracellular ROS, 5  $\mu$ M Cell ROX green reagent (ThermoFisher Scientific, C10444) was loaded to bacteria infected A549 cells for 30 min followed by fixation using 4% paraformaldehyde. Cells were immunostained using anti-Legionella antibody and imaged using the 488 nm laser line and 40X objective of the Zeiss LSM780 system. All imaging parameters (laser power, magnification and gain settings) were kept identical to compare intensities between samples. Images were analyzed in FIJI by measuring 488 nm (green) signal collected from the infected cells marked manually as multiple regions of interest (ROIs). 100 cells per set were analyzed per set taken from 3 experiments.

### Redox GFP measurements

Redox GFP (roGFP) targeted to the mitochondrial matrix or cytosolic redox GFP was transfected in A549 cells 24 h prior to bacterial infection. Cells were infected with Legionella for different lengths of time and imaged using confocal imaging. For microscopy, excitation wavelengths of 365 nm, and 488 nm were used sequentially. In both cases emission signals were collected using the GFP filter (emission maxima 510 nm). Oxidized roGFP is excited at 365 nm while the reduced form of is excited at 470 nm. Z-stacks with 0.5  $\mu$ m slices were imaged for at least 60 cells taken from 3 experiments and analyzed in FIJI as before [40]. Briefly, images were converted to 32-bit, background subtracted, thresholded and the 'image calculator' was used to divide the signal from oxidized roGFP (365 nm excitation) by reduced roGFP (Excitation 488 nm). This ratio was calculated from each of the 60 cells and plotted in the online tool for boxplot generation boxplotR (<http://shiny.chemgrid.org/boxplotr/>)

### Luciferase activity assay

To analyze the induction of NFE2L2-induced genes, a luciferase reporter assay was used in A549 cells. In brief, an expression construct containing the luciferase ORF and the NFE2L2 promoter with antioxidant response element (NFE2L2-ARE) was transfected. In total, 100 ng plasmid was used per one well of a 12-well dish. All transfections were performed in triplicate and the average of three experiments is shown in figures. Sixteen hours after transfection, cells were infected with bacteria for indicated timespans. Luciferase expression was measured using the Luciferase Reporter Assay System (Promega, E1500). Fold change was calculated by taking untreated cells as 1.

### Statistical analysis

All experiments were performed at least 3 times with similar results. For western blotting, band intensities were quantified in Bio-Rad Image Lab 6.1 software. Immunoprecipitations were normalized to the bait protein while lysates were normalized to GAPDH. Error bars indicate standard deviations. For immunofluorescence experiments, intensities were measured in FIJI taking at least 60 cells from 3 independent experiments. Box-plots were drawn in BoxplotR. For box-plots, center lines show medians, box limits indicate the 25<sup>th</sup> and 75<sup>th</sup> percentile as determined by R software, whiskers

extend 1.5 times the interquartile range from the 25<sup>th</sup> and 75<sup>th</sup> percentiles, outliers are represented by dots. Number of cells (n) is mentioned in figure legends. *p* values were calculated in MS Excel using Students *t*-test (2 tailed, type 3).

### Nuclear fractionation

A549 cells from a confluent 60-mm dish transiently transfected MYC-NFE2L2. 16 h later they are infected with Legionella strains for 6 h. Cells were lysed in 300  $\mu$ L of hypotonic buffer (10 mM HEPES, pH 7.4, 2 mM MgCl<sub>2</sub>, 25 mM KCl, 1 mM DTT, 1 mM PMSF [Sigma, P7626], and protease inhibitor cocktail [Roche 11,836,170,001]), kept on ice for 30 min followed by syringe lysis, then 125  $\mu$ L of a 2 M sucrose (Sigma, S0389) solution was added dropwise, followed by centrifugation at 1000 g for 15 min. The supernatant was saved as the cytosolic fraction. The pellet was washed twice in wash buffer (10 mM HEPES, pH 7.4, 2 mM MgCl<sub>2</sub>, 25 mM KCl, 250 mM sucrose, 1 mM DTT, 1 mM PMSF, and protease inhibitor cocktail) and saved as the nuclear fraction.

### NFE2L2 ubiquitination assay

A549 cells expressing MYC-NFE2L2 were infected with Legionella for 6 and treated with 20  $\mu$ M MG132 2 h prior to lysis. Cells were lysed in 50 mM Tris (pH 7.5), 150 mM NaCl, 2% SDS and 10 mM *N*-ethylmaleimide (Sigma, E3876). Lysates were diluted fivefold in buffer containing 50 mM Tris-HCl, pH 7.5, 150 mM NaCl, 1% Triton X-100. Lysates were incubated with MYC agarose resin for two h at 4°C, followed by washing in wash buffer containing 50 mM Tris-HCl, pH 7.5, 400 mM NaCl and 1% Triton X-100. Samples were analyzed by SDS gel electrophoresis, transferred to PVDF membranes, and immunoblotted with the anti-Ub, and MYC antibodies.

### TUBE2 enrichment of polyubiquitinated proteins

Cells after infection were treated with 10  $\mu$ M MG132 for 2 h prior to lysis. Cells were lysed in lysis buffer (50 mM Tris, pH 8, 150 mM NaCl, 1% Triton X-100, protease inhibitor and 10 mM *N*-ethylmaleimide). Lysate containing 200  $\mu$ g protein was incubated with 10  $\mu$ L TUBE2 agarose resin (Life Sensors, 182UM402) overnight at 4°C. Resin was washed thrice in wash buffer (50 mM Tris, pH 8, 300 mM NaCl, 0.1% Triton X-100, protease inhibitor and 1 mM NEM) and heated with 30  $\mu$ L of 2 $\times$  Laemmli's sample buffer followed by western blotting.

### Quantification of cellular RNA

For real time PCR, total RNA was isolated using Trizol according to the manufacturer's instructions (Invitrogen 15,596,026). In total, 1  $\mu$ g RNA was converted to cDNA using random hexamer primer using Thermo cDNA synthesis kit. RT-PCR was performed using EvaGreen (Biotium 89,138-982) and the Bio-Rad CFX Connect Real-time PCR system. Gene expression was compared using *C<sub>t</sub>* values and the results were calculated using  $\Delta\Delta C_t$  method with normalization to the average expression level of RNA18S/18S rRNA. Forward (F) and reverse (R) primers used are as follows:

Gene	Forward primer	Reverse primer
NFE2L2	5'-CAGCGACGGAAAGAGTATGA-3'	5'-TGGGCAACCTGGGAGTAG-3'
SQSTM1	5'-TGCCAGACTACGACTTGTG-3'	5'-AGTGTCCGTGTTTCACCTCC-3'
HMOX1	5'-CAACATCCAGCTCTTTGAGG-3'	5'-GGCAGAATCTTGCACTTTG-3'
TXNRD1	5'-CCACTGGTGAAAGACCACGTT-3'	5'-AGGAGAAAAGATCATCACTGCTGAT-3'
NQO1	5'-AGCCAGATATTGTGGCCG-3'	5'-CCTTTCAGAATGGCTGGCAC-3'
SOD2	5'-CTGATTTGGACAAGCAGCAA-3'	5'-CTGGACAAACCTCAGCCCTA-3'
RNA18S rRNA	5'-AAACGGCTACCACATCCAAG-3'	5'-CAATTACAGGGCCTCGAAAG-3'

## RNA sequencing

50 µg RNA was isolated using the Qiagen mRNA isolation kit (Qiagen 74,104). Quality of RNA was assessed by checking on an agarose gel to see the intactness of the *RNA28S*, and *RNA18S* rRNA bands and absorbance at 260 nm and 280 nm was measured by Nanodrop. Absorbance(260 nm: 280 nm) was > 1.8, and Absorbance(260 nm: 230 nm) > 2.0. Isolated RNA was used for next generation RNA sequencing using Illumina platform. Data was analyzed by ROSALIND® (<https://rosalind.bio/>), with a HyperScale architecture developed by ROSALIND, Inc. (San Diego, CA). Reads were trimmed using cutadapt [41]. Quality scores were assessed using FastQC [42]. Reads were aligned to the *Homo sapiens* genome build GRCh38 using STAR [43]. Individual sample reads were quantified using HTseq [44] and normalized via Relative Log Expression (RLE) using DESeq2 R library [45]. Normalized expression of genes between 4 replicates each of WT, ΔS and non-infected cells were compared. Students t test (2 tailed type 3) was used to calculate *p* values. Volcano plots were generated to visualize differential gene expression between WT and ΔS Legionella infection.

## Sample preparation for mass spectrometry

A549 cells were infected with Legionella for 6 h in the presence of tBHQ (10 µM; MedChemExpress, HY-100489) or ML385 (10 µM; MedChemExpress, HY-100523). Cells were lysed in SDS-lysis buffer (50 mM Tris, 2% SDS, 10 mM TCEP [Sigma 646,547], 40 mM chloroacetamide [Sigma, C0267], protease inhibitor cocktail, phosphatase inhibitor [Sigma, PHOSS-RO]) heated to 95°C for 10 min. Proteins were precipitated using methanol-chloroform precipitation and resuspended in 8 M urea. Isolated proteins were digested with 1:50 w:w LysC (Wako Chemicals, NC9223464); cleaves at the carboxylic side of lysine residue) and 1:100 w:w trypsin (Promega, V5280); cleaves at the carboxylic side of lysine and arginine residues) overnight at 37°C after dilution to a final urea concentration of 1 M. Digests were then acidified (pH 2–3) using trifluoroacetic acid (TFA). Peptides were purified using C18 SepPak columns (Waters, WAT036945). Desalted peptides were dried and 25 µg of peptides was resuspended in TMT-labeling buffer (200 mM EPPS [Sigma, WAT036945], pH 8.2, 20% acetonitrile). Peptides (160 µg) were subjected to TMT labeling (Thermo Scientific 90,061) with 1:2 peptide TMT ratio (w:w) for 1 h at room temperature. The labeling reaction was quenched by addition of hydroxylamine to a final concentration of 0.5% and incubation at room temperature for an additional 15 min.

## Mass spectrometric data acquisition

Samples were pooled in equimolar ratio and subjected to High pH Reversed-Phase Peptide Fractionation kit (Thermo Fisher Scientific 84,868) following the manufacturer's instructions. Eluted fractions were dried in SpeedVac and peptides were resuspended in 3% acetonitrile:0.1% TFA for liquid chromatography – mass spectrometry. All mass spectrometry data was acquired in centroid mode on an Orbitrap Fusion Lumos mass spectrometer hyphenated to an easy-nLC 1200 nano HPLC system with a nanoFlex ion source (Thermo Fisher Scientific). Resuspended peptides were separated on an Easy nLC 1200 (Thermo Fisher Scientific) and a 22-cm-long, 75-µm-innerdiameter fused-silica column, which had been packed in house with 1.9-µm C18 particles (ReproSil-Pur; Dr Maisch, r1.b9) and kept at 45°C using an integrated column oven (Sonation). Peptides were eluted by a nonlinear gradient from 8 to 60% acetonitrile over 155 min followed by an increase to 95%B in 1 min, which was held for another 10 min. Full-scan MS spectra (350–1400 m/z) were acquired at a resolution of 120,000 at m/z 200, a maximum injection time of 100 ms, and an AGC target value of  $4 \times 10^5$ . Up to 20 most intense precursors, with charge state in between 2 and 5, were isolated using a 0.7 Th window. MS/MS spectra were acquired with a maximum injection time of 50 ms, AGC target value of  $1.5 \times 10^4$ , and fragmented using CID with a normalized collision energy of 35%. SPS-MS3 scans were done on the ten most intense MS2 fragment ions having an isolation window of 0.7 Th (MS) and 2 m/z (MS2). Ions were fragmented using NCE of 50% and analyzed in the orbitrap with the resolution of 50,000 at m/z 200, scan range 110–500 m/z, AGC target value  $1.5 \times 10^5$ , and a maximum injection time of 120 ms.

## Mass spectrometric data analysis

Raw mass spectrometry data were analyzed with Proteome Discoverer (v.2.4, Thermo Fisher Scientific) using Sequest HT as a search engine and performing recalibration of precursor masses by the Spectrum RC-node. Number of missed cleavages permitted was 2. Mass tolerance of precursor ions is 7 ppm and mass tolerance of fragment ions is 0.5 Da. Fragment spectra were searched against the human reference proteome (“one sequence per gene,” 20531 sequences, version March 2020) downloaded from Uniprot in March 2020, as well as common contaminants as included in “contaminants.fasta” provided with the MaxQuant software (version 1.6.11). Static modifications were TMT at the peptide N terminus and lysines as well as carbamidomethyl at cysteine residues, dynamic modifications were set as oxidation of methionine



and acetylation at the protein N terminus. Matched spectra were filtered with Percolator, applying a false discovery rate of 1% on peptide spectrum match and protein level. Reporter intensities were normalized to the total protein intensities in Proteome Discoverer, assuming equal sample loading and additionally by median normalization using the NormalyzerDE package. Statistically significant changes between samples were determined in Perseus (v.1.6.6.0). Data set was first filtered for contaminants and biological replicates were grouped as one. Proteins were further filtered for two valid values present in at least one group. Missing values were imputed from normal distribution of data using default settings. Significant candidates were chosen using two-sided *t* test with error-corrected *p*-values (0.01, FDR) and log<sub>2</sub> (fold change) value minimum of  $\pm 0.5$ . To avoid false-positive protein identification,  $\geq 2$  unique peptides identified within a single protein were used for further analysis. Network and gene ontology analysis was performed with statistically significant hits using the online Metascape software

## Acknowledgements

We would like to thank Florian Bonn for his help with the DSF mass spectrometric determination of PR-Ub sites.

## Disclosure statement

No potential conflict of interest was reported by the author(s).

## Funding

The work was supported by the Alexander von Humboldt-Stiftung Deutsche Forschungsgemeinschaft [Project-ID 323732846, Project-ID 25913077-SFB1177.]; EMBO post-doctoral fellowship (ALTF 199-2021) Korea government and the Yonsei University Research Fund of 2021 (2021-22-0050) (MSIT) [No. 2021R1C1C1003961].

## Data availability statement

Mass spectrometric data pertaining to proteome changes in Legionella infection available upon request.

## ORCID

Ivan Dikic  <http://orcid.org/0000-0001-8156-9511>

## References

- [1] Kobayashi A, Kang MI, Okawa H, et al. Oxidative stress sensor KEAP1 functions as an adaptor for Cul3-based E3 ligase to regulate proteasomal degradation of NRF2. *Mol Cell Biol.* 2004;24(16):7130–7139. doi: 10.1128/MCB.24.16.7130-7139.2004
- [2] Danieli A, Martens S. SQSTM1-mediated phase separation at the intersection of the ubiquitin-proteasome system and autophagy. *J Cell Sci.* 2018;131(19):jcs214304. doi: 10.1242/jcs.214304
- [3] Herhaus L, Dikic I. Ubiquitin-induced phase separation of SQSTM1/SQSTM1. *Cell Res.* 2018;28(4):389. doi: 10.1038/s41422-018-0030-x
- [4] Sánchez-Martín P, Saito T, Komatsu M. p62/SQSTM1: 'Jack of all trades' in health and cancer. *FEBS J.* 2019;286(1):8–23. doi: 10.1111/febs.14712
- [5] Komatsu M, Kurokawa H, Waguri S, et al. The selective autophagy substrate SQSTM1 activates the stress responsive transcription factor NRF2 through inactivation of KEAP1. *Nat Cell Biol.* 2010;12(3):213–223. doi: 10.1038/ncb2021
- [6] Ichimura Y, Waguri S, Sou YS, et al. Phosphorylation of p62 activates the KEAP1-NRF2 pathway during selective autophagy. *Mol Cell.* 2013;51(5):618–631. doi: 10.1016/j.molcel.2013.08.003
- [7] Katsuragi Y, Ichimura Y, Komatsu M. p62/SQSTM1 functions as a signaling hub and an autophagy adaptor. *FEBS J.* 2015;282(24):4672–4678. doi: 10.1111/febs.13540
- [8] Yang Y, Willis TL, Button RW, et al. Cytoplasmic DAXX drives p62/SQSTM1 phase condensation to activate NRF2-mediated stress response. *Nat Commun.* 2019;10(1):3759. doi: 10.1038/s41467-019-11671-2
- [9] Kageyama S, Gudmundsson SR, Sou YS, et al. p62/SQSTM1-droplet serves as a platform for autophagosome formation and anti-oxidative stress response. *Nat Commun.* 2021;12(1):16. doi: 10.1038/s41467-020-20185-1
- [10] Komatsu M. p62 bodies: phase separation, NRF2 activation, and selective autophagic degradation. *IUBMB Life.* 2022;74(12):1200–1208. doi: 10.1002/iub.2689
- [11] Nairz M, Schleicher U, Schroll A, et al. Nitric oxide-mediated regulation of ferroportin-1 controls macrophage iron homeostasis and immune function in Salmonella infection. *J Exp Med.* 2013;210(5):855–873. doi: 10.1084/jem.20121946
- [12] Harvey CJ, Thimmulappa RK, Sethi S, et al. Targeting NRF2 signaling improves bacterial clearance by alveolar macrophages in patients with COPD and in a mouse model. *Sci Transl Med.* 2011;3(78):ra7832–ra7832. doi: 10.1126/scitranslmed.3002042
- [13] MacGarvey NC, Suliman HB, Bartz RR, et al. Activation of mitochondrial biogenesis by heme oxygenase-1-mediated NF-E2-related factor-2 induction rescues mice from lethal staphylococcus aureus sepsis. *Am J Respir Crit Care Med.* 2012;185(8):851–861. doi: 10.1164/rccm.201106-1152OC
- [14] Winchell CG, Dragan AL, Brann KR, et al. Coxiella burnetii subverts SQSTM1/sequestosome 1 and activates NRF2 signaling in human macrophages. *Infect Immun.* 2018;86(5):e00608–17. 29483292. doi: 10.1128/IAI.00608-17
- [15] Rothchild AC, Olson GS, Nemeth J, et al. Alveolar macrophages generate a noncanonical NRF2-driven transcriptional response to mycobacterium tuberculosis in vivo. *Sci Immunol.* 2019;4(37):eaaw6693. doi: 10.1126/sciimmunol.aaw6693
- [16] Qiu J, Sheedlo MJ, Yu K, et al. Ubiquitination independent of E1 and E2 enzymes by bacterial effectors. *Nature.* 2016;533(7601):120–124. doi: 10.1038/nature17657
- [17] Bhogaraju S, Kalayil S, Liu Y, et al. Phosphoribosylation of ubiquitin promotes serine ubiquitination and impairs conventional ubiquitination. *Cell.* 2016;167(6):1636–1649. doi: 10.1016/j.cell.2016.11.019
- [18] Kotewicz KM, Ramabhadran V, Sjoblom N, et al. A single Legionella effector catalyzes a multistep ubiquitination pathway to rearrange tubular endoplasmic reticulum for replication. *Cell Host & Microbe.* 2017;21(2):169–181. doi: 10.1016/j.chom.2016.12.007
- [19] Akturk A, Wasilko DJ, Wu X, et al. Mechanism of phosphoribosyl-ubiquitination mediated by a single legionella effector. *Nature.* 2018;557(7707):729–733. doi: 10.1038/s41586-018-0147-6
- [20] Dong Y, Mu Y, Xie Y, et al. Structural basis of ubiquitin modification by the legionella effector SdeA. *Nature.* 2018;557(7707):674–678. doi: 10.1038/s41586-018-0146-7
- [21] Kalayil S, Bhogaraju S, Bonn F, et al. Insights into catalysis and function of phosphoribosyl-linked serine ubiquitination. *Nature.* 2018;557(7707):734–738. doi: 10.1038/s41586-018-0145-8
- [22] Shin D, Mukherjee R, Liu Y, et al. Regulation of phosphoribosyl-linked serine ubiquitination by deubiquitinases DupA and DupB. *Molecular Cell.* 2020;77(1):164–179. doi: 10.1016/j.molcel.2019.10.019

- [23] Bhogaraju S, Bonn F, Mukherjee R, et al. Inhibition of bacterial ubiquitin ligases by SidJ–calmodulin catalysed glutamylation. *Nature*. 2019;572(7769):382–386. doi: [10.1038/s41586-019-1440-8](https://doi.org/10.1038/s41586-019-1440-8)
- [24] Black MH, Osinski A, Gradowski M, et al. Bacterial pseudokinase catalyzes protein polyglutamylation to inhibit the SidE-family ubiquitin ligases. *Science*. 2019;364(6442):787–792. doi: [10.1126/science.aaw7446](https://doi.org/10.1126/science.aaw7446)
- [25] Gan N, Zhen X, Liu Y, et al. Regulation of phosphoribosyl ubiquitination by a calmodulin-dependent glutamylase. *Nature*. 2019;572(7769):387–391. doi: [10.1038/s41586-019-1439-1](https://doi.org/10.1038/s41586-019-1439-1)
- [26] Liu Y, Mukherjee R, Bonn F, et al. Serine-ubiquitination regulates Golgi morphology and the secretory pathway upon legionella infection. *Cell Death Differ*. 2021;28(10):2957–2969. doi: [10.1038/s41418-021-00830-y](https://doi.org/10.1038/s41418-021-00830-y)
- [27] Choy A, Dancourt J, Mugo B, et al. The legionella effector RavZ inhibits host autophagy through irreversible Atg8 deconjugation. *Science*. 2012;338(6110):1072–1076. doi: [10.1126/science.1227026](https://doi.org/10.1126/science.1227026)
- [28] Yang A, Pantoom S, Wu YW. Elucidation of the anti-autophagy mechanism of the legionella effector RavZ using semisynthetic LC3 proteins. *Elife*. 2017;6:e23905. doi: [10.7554/eLife.23905](https://doi.org/10.7554/eLife.23905)
- [29] Han H, Cho JW, Lee S, et al. TRRUST v2: an expanded reference database of human and mouse transcriptional regulatory interactions. *Nucleic Acids Res*. 2018;46(D1):D380–D386. doi: [10.1093/nar/gkx1013](https://doi.org/10.1093/nar/gkx1013)
- [30] Omotade TO, Roy CR, Brodsky IE. Legionella pneumophila excludes autophagy adaptors from the ubiquitin-labeled vacuole in which it resides. *Infect Immun*. 2020;88(8):10–1128. doi: [10.1128/IAI.00793-19](https://doi.org/10.1128/IAI.00793-19)
- [31] Escoll P, Song OR, Viana F, et al. Legionella pneumophila modulates mitochondrial dynamics to trigger metabolic repurposing of infected macrophages. *Cell Host & Microbe*. 2017;22(3):302–316. doi: [10.1016/j.chom.2017.07.020](https://doi.org/10.1016/j.chom.2017.07.020)
- [32] Cuadrado A, Martín-Moldes Z, Ye J, et al. Transcription factors NRF2 and nf-κB are coordinated effectors of the rho family, gtp-binding protein RAC1 during inflammation. *J Biol Chem*. 2014;289(22):15244–15258. doi: [10.1074/jbc.M113.540633](https://doi.org/10.1074/jbc.M113.540633)
- [33] Brazão V, Colato RP, Santello FH, et al. Melatonin regulates antioxidant defense and inflammatory response by activating NRF2-dependent mechanisms and inhibiting NFκB expression in middle-aged T. cruzi infected rats. *Exp Gerontol*. 2022;167:111895. doi: [10.1016/j.exger.2022.111895](https://doi.org/10.1016/j.exger.2022.111895)
- [34] Wu J, Li S, Li C, et al. The non-canonical effects of heme oxygenase-1, a classical fighter against oxidative stress. *Redox Biol*. 2021;47:102170. doi: [10.1016/j.redox.2021.102170](https://doi.org/10.1016/j.redox.2021.102170)
- [35] Joshi CS, Mora A, Felder PA, et al. NRF2 promotes urothelial cell response to bacterial infection by regulating reactive oxygen species and RAB27B expression. *Cell Rep*. 2021;37(3):109856. doi: [10.1016/j.celrep.2021.109856](https://doi.org/10.1016/j.celrep.2021.109856)
- [36] Furukawa M, Xiong Y. BTB protein KEAP1 targets antioxidant transcription factor NRF2 for ubiquitination by the cullin 3-Roc1 ligase. *Mol Cell Biol*. 2005;25(1):162–171. doi: [10.1128/MCB.25.1.162-171.2005](https://doi.org/10.1128/MCB.25.1.162-171.2005)
- [37] Waypa GB, Marks JD, Mack MM, et al. Hypoxic pulmonary vasoconstriction: redox events in oxygen sensing. *J Appl Physiol*. 2005;98(1):404–414. doi: [10.1152/jappphysiol.00722.2004](https://doi.org/10.1152/jappphysiol.00722.2004)
- [38] O’Connell DJ, Kolde R, Sooknah M, et al. Simultaneous pathway activity inference and gene expression analysis using RNA sequencing. *Cell Syst*. 2016;2(5):323–334. doi: [10.1016/j.cels.2016.04.011](https://doi.org/10.1016/j.cels.2016.04.011)
- [39] Leidecker O, Bonfiglio JJ, Colby T, et al. Serine is a new target residue for endogenous adp-ribosylation on histones. *Nat Chem Biol*. 2016;12(12):998–1000. doi: [10.1038/nchembio.2180](https://doi.org/10.1038/nchembio.2180)
- [40] Vevea JD, Wolken DMA, Swayne TC, et al. Ratiometric biosensors that measure mitochondrial redox state and ATP in living yeast cells. *J Vis Exp*. 2013;77(77):e50633. doi: [10.3791/50633-v](https://doi.org/10.3791/50633-v)
- [41] Martin M. Cutadapt removes adapter sequences from high-throughput sequencing reads. *EMBnet J*. 2011;17(1):10–12. doi: [10.14806/ej.17.1.200](https://doi.org/10.14806/ej.17.1.200)
- [42] Andrews S. FastQC: a quality control tool for high throughput sequence data. 2010. Available from: <https://www.bioinformatics.babraham.ac.uk/projects/fastqc/>
- [43] Dobin A, Davis CA, Schlesinger F, et al. STAR: ultrafast universal RNA-seq aligner. *Bioinformatics*. 2013;29(1):15–21. doi: [10.1093/bioinformatics/bts635](https://doi.org/10.1093/bioinformatics/bts635)
- [44] Anders S, Pyl PT, Huber W. Htseq—a Python framework to work with high-throughput sequencing data. *Bioinformatics*. 2015;31(2):166–169. doi: [10.1093/bioinformatics/btu638](https://doi.org/10.1093/bioinformatics/btu638)
- [45] Love MI, Huber W, Anders S. Moderated estimation of fold change and dispersion for rna-seq data with DESeq2. *Genome Biol*. 2014;15(12):1–21. doi: [10.1186/s13059-014-0550-8](https://doi.org/10.1186/s13059-014-0550-8)